Turning the band alignment of carbon dots for visible-light-driven enzymatic asymmetric reduction of aromatic ketone

Qiao, Li; Ma, Bianqin; Jiang, Yongjian; Pan, Xiaoting; Mao, Zhili; Zhang, Yi; Sheldon, Roger A.; Wang, Anming

DOI
10.1016/j.ijbiomac.2024.139444

Publication date
2025

Document Version
Final published version

Published in
International Journal of Biological Macromolecules

Citation (APA)
Qiao, L., Ma, B., Jiang, Y., Pan, X., Mao, Z., Zhang, Y., Sheldon, R. A., & Wang, A. (2025). Turning the band alignment of carbon dots for visible-light-driven enzymatic asymmetric reduction of aromatic ketone. *International Journal of Biological Macromolecules*, *295*, Article 139444. https://doi.org/10.1016/j.ijbiomac.2024.139444

International Journal of Biological Macromolecules 295 (2025) 139444

Contents lists available at ScienceDirect

International Journal of Biological Macromolecules

journal homepage: www.elsevier.com/locate/ijbiomac

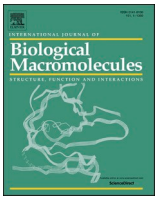

Turning the band alignment of carbon dots for visible-light-driven enzymatic asymmetric reduction of aromatic ketone

Li Qiao [a,b], Bianqin Ma [b], Yongjian Jiang [b], Xiaoting Pan [b], Zhili Mao [b], Yi Zhang [a,*], Roger A. Sheldon [c,d,**], Anming Wang [b,*]

[a] Hunan Provincial Key Laboratory of Micro & Nano Materials Interface Science, College of Chemistry and Chemical Engineering, Central South University, Changsha 410083, PR China
[b] Key Laboratory of Organosilicon Chemistry and Materials Technology, Ministry of Education; College of Materials Chemistry and Chemical Engineering, Hangzhou Normal University, Hangzhou, Zhejiang 311121, China
[c] Molecular Sciences Institute, School of Chemistry, University of the Witwatersrand, PO Wits, 2050 Johannesburg, South Africa
[d] Department of Biotechnology, Section BOC, Delft University of Technology, van der Maasweg 9, 2629, HZ, Delft, the Netherlands

ARTICLE INFO

Keywords:
Bio-photo-hybridization system
Photo-enzymatic catalysis
Chiral alcohol
Aldo-keto reductase

ABSTRACT

Keto reductases are crucial NAD(*P*)H-dependent enzymes used for the enantioselective synthesis of alcohols from prochiral ketones. Typically, the NADPH cofactor is regenerated through a second enzyme and/or substrate. However, photocatalytic cofactor regeneration using water as a sacrificial electron and hydrogen donor presents a promising alternative, albeit a challenging one. Herein we fabricated several nitrogen-doped carbon dots (CDs) with visible light absorption properties, good water solubility and biocompatibility for photocatalytic regeneration of NADPH. The CD with a smaller size and suitable redox potential gave the highest NADPH yield (55.7 %). Based on this, NADPH-dependent aldo-keto reductase crosslinked aggregates (AKR-CLEs) were initially applied as a stable biocatalyst to reduce the prochiral ketone. (*S*)-1-(2-Chlorophenyl) ethanol, an intermediate for LPA1R antagonists, was obtained in 65.3 % yield and 99.99 % enantiomeric excess (ee) under visible light irradiation. The isotope tracer experiment confirmed that water is the hydrogen donor in this light-driven, photo-enzymatic asymmetric hydrogenation system. This method is useful for the sustainable synthesis of chiral alcohols. Moreover, the general principle of utilizing water as the sacrificial hydrogen and electron donor holds potential for application in other redox cofactor regeneration systems.

1. Introduction

Enzyme-catalyzed reactions are characterized by high efficiency, specificity, and high (*enantio*)selectivity [1]. However, for large-scale applications [2], most of these reactions require a cofactor regeneration system [3–5]. Such systems can be divided into four categories: enzymatic regeneration, chemical regeneration, electrochemical regeneration, and photocatalytic regeneration [6]. Photocatalytic regeneration, which mimics natural photosynthesis by converting light energy into chemical energy eliminating the need for a second enzyme and co-substrate, such as formate dehydrogenase (FDH) / formate, glucose dehydrogenase (GDH) / glucose or alcohol dehydrogenase (ADH) / alcohol [7–9].

The bio-photo-hybridization system, comprising light-trapping elements and biocatalysts, can efficiently harvest light and perform highly enantioselective reduction of prochiral ketones [10–12]. In this system, the photosensitizer excites hole-electron pairs under light irradiation. Electrons are transferred to the hydride transfer catalyst, while holes participate in oxidation, enabling realizing redox cycling photocatalysis [13]. Photocatalytic NAD(*P*)H regeneration requires proton and electrons from a sacrificial hydride donor [14–16], such as triethanolamine (TEOA) [17–19], ethylenediaminetetraacetic acid (EDTA) [20] and ascorbic acid (AA) [21]. However, using these valuable chemicals results in waste generation, and complicated separation, and can destroy enzyme activity [6].

In contrast, water as a sacrificial hydrogen donor minimizes waste and reduces costs, though there are limited reports on this approach. Hollmann et al. investigated water-oxidizing catalysts for electron

* Corresponding authors.
** Corresponding author at: Molecular Sciences Institute, School of Chemistry, University of the Witwatersrand, PO Wits, 2050 Johannesburg, South Africa.
E-mail addresses: yzhangcsu@csu.edu.cn (Y. Zhang), roger.sheldon@wits.ac.za (R.A. Sheldon), waming@hznu.edu.cn (A. Wang).

https://doi.org/10.1016/j.ijbiomac.2024.139444
Received 1 October 2024; Received in revised form 31 December 2024; Accepted 31 December 2024
Available online 4 January 2025

supply for ene-reductases. They regenerated NAD(*P*)H through water oxidation under UV and visible light using a titanium dioxide-based photocatalyst and facilitated protons and electrons transfer *via* a flavin cofactor to the ene-reductase, demonstrating water's potential as a sacrificial electron donor in biocatalytic redox reactions [22]. Furthermore, Hollmann et al. engineered enoate reductase to be expressed in cyanophyta, a single-celled prokaryote known for oxygen-releasing photosynthesis, for the asymmetric reduction of C═C bonds driven by biocatalytic oxidation of water [23]. Employing water as a stoichiometric reductant eliminates the need for additional sacrificial hydrogen donors, thus reducing unwanted by-products. This reaction achieves efficiency comparable to traditional whole-cell biotransformations in *E. coli*, yielding optically pure 2-methylsuccinimide (99 % ee, 80 % yield) from 100 mg of the prochiral 2-methylmaleimide solution under optimized conditions. Reisner et al. used a semi-artificial approach to study photobiological water splitting by directly coupling the water oxidation enzyme, photosystem II, with the H_2 evolving enzyme, hydrogenase [24]. By incorporating enzymes into an artificial photochemical cell, they developed a custom-layered indium tin oxide electrode, enabling the effective integration of photosystem II at the anode and hydrogenase at the cathode, achieving efficient half-reactions for water-splitting.

Developing photocatalysts with water oxidation capabilities is highly desirable but presents significant challenges [25–28]. Since enzymes are prone to inactivation, the bio-photo-hybridization system must operate under mild conditions, and the photosensitizers used in photocatalytic half-reactions must be non-toxic and biocompatible [29–31]. Carbon dots (CDs) are polycyclic aromatic hydrocarbons containing various hydrophilic functional groups, with diameters ranging from a few to tens of nanometers [32]. Compared with other semiconductor materials, CDs offer advantages such as low cost, easy modification, and good water solubility [33–35]. Notably, CDs with smaller sizes and changeable properties exhibit desirable good optical and electronic behavior, making them widely used in photocatalysis [36,37]. However, the photocatalytic capacity of CDs is limited by their weak photo-redox potentials. CDs often functioned as co-catalysts to reduce band gap energy, broaden light absorption range, and improve charge carrier transfer efficiency when incorporated into the structure of photocatalysts like TiO_2 [38,39].

Core nitrogen doping in CDs has significant effects in the context of photocatalysis by modifying energy levels or enhancing the efficiency of charge transfer reactions [40–42]. The presence of nitrogen improves charge delocalization and reduces the work function, and energy transfer processes in CD nanomaterials, making them suitable as photocatalytic additives [43]. Fundamentally, their photocatalytic properties are closely related to band alignment. A variety of organic materials have been used for CD preparations. Among these, perylene-based polycyclic aromatic hydrocarbon precursors provide CDs with increased π-conjugation, making them promising materials for photocatalytic applications [44,45].

In this work, we explored the preparation of CDs using perylene-3,4,9,10-tetracarboxylic dianhydride (PTCDA) as a precursor to obtain hydrophilic materials with multi-conjugated structures, capable of photosplitting water for cofactor regeneration. Besides, we designed a series of CDs by varying the nitrogen and carbon sources, as well as adjusting the reaction conditions. An autarkic cofactor "one-pot" cascade system was designed for photo-enzymatic catalysis, using AKR as a model enzyme to reduce prochiral ketones for the synthesis of chiral alcohols (Scheme 1). The photocatalytic performance of CDs was evaluated based on the conversion of aromatic ketone. Furthermore, the photocatalytic mechanism of CDs was discussed, and the reasons for the observed differences in photocatalytic efficiency were analyzed. This study bridges the gap between CDs and enzyme catalysis, offering a green and sustainable system for enzyme-catalyzed synthesis of chiral alcohols.

2. Materials and methods

2.1. Materials and instrumentation

All chemicals were procured and utilized as received, without any additional purification. Perylene-3,4,9,10-tetracarboxylic dianhydride (PTCDA, 98 %), urea (>99 %), sodium citrate, citric acid (99.5 %), rhodium(III) trichloride hydrate ($RhCl_3{\cdot}3H_2O$, 98 %), ethylene diamine tetraacetic acid (EDTA), 3,5-bis(trifluoromethyl)acetophenone (98 %), and 1,2,3,4,5-pentamethylcyclopentadiene (95 %) were purchased from Shanghai Aladdin Bio-Chem Technology Co., Ltd., Shanghai, China. Dibenzocycloocta-4a,6a-diene-5,11-diyne (DBA, 99 %), sodium chloride (NaCl, AR), zinc acetate [$Zn(OAc)_2$, AR], hydrochloric acid (HCl, 37 %), β-nicotinamide adenine dinucleotide sodium salt ($NADP^+$, 95 %), dichloromethane (CH_2Cl_2, AR), sodium sulfate (Na_2SO_4, AR), *o*-chloroacetophenone (98 %), (*S*)-1-(2-chlorophenyl) ethanol (98 %), (*R*)-1-[3,5-bis(trifluoromethyl)phenyl]ethanol (>99 %), 3-chloro-1-phenylpropan-1-one (98 %), (*S*)-3-chloro-1-phenylpropan-1-ol (99 %) and methyl alcohol (MeOH, AR) originated from Senrise Bio-Chem Technology Co., Ltd., Shanghai, China. The strains *Escherichia coli* DH5α used in the study were ordered from Stratagene. *E. coli* C321.ΔA. and plasmids (pZE21-GFPaav and pEVOL-*p*AzF) were obtained from Addgene, where the AKR gene was kept from our laboratory.

High-resolution transmission electron microscope (HRTEM, JEOL JEM-2100F operated at 200 kV) and confocal laser scanning microscopy (CLSM, Zeiss LSM 900, Airy Scan 2) were used for morphological studies. The UV¯vis absorption spectra were collected on a UV¯vis-NIR spectrophotometer (SHIMADZU-UV-1900i), and the photoluminescence spectra (PL spectra) of all nanomaterials were collected at room temperature on a Hitachi F-7000 Flourescence Spectrophotometer. Quantum yield (QY) and time-resolved photoluminescence (TRPL) spectra were measured on a steady state/transient fluorescence spectrometer

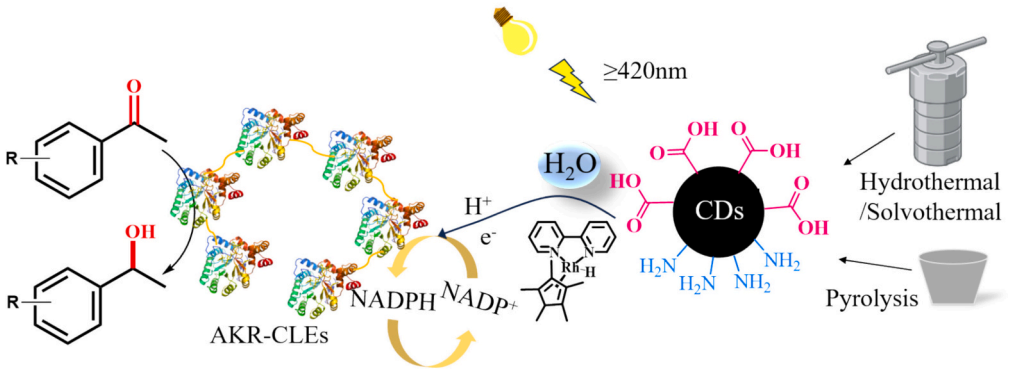

Scheme 1. Schematic representation of enzyme¯carbon dots-hybrid system for synthesis of chiral aromatic ethanol.

(FLS 980-STM). X-ray photoelectron spectroscopy (XPS) measurements were performed using an electron analyzer (Thermo Scientific K-Alpha, US). We collected the Raman spectra on a Raman spectroscope (Horiba LabRAM HR Evolution, Japan) equipped with autofocus and fast spectral imaging module. The spectroscope has a focal length of 800 mm and the exciter wavelength is selected at 785 nm. The crystal structure of CDs was characterized by powder X-ray diffraction (XRD) by using an D8ADVANCE (Bruker) X-ray diffractometer with Cu Kα radiation (λ = 0.154178 nm). Molecular weights were tested by high-resolution liquid chromatography-triple quadrupole-time of flight mass spectrometer.

2.2. Prepare and characterization of carbon dots (CDs) and calculating

CDs with different band alignments were prepared by aggregating the corresponding carbon and nitrogen sources through various methods.

To synthesize PT-NCDs, a mixture of 0.4 g PTCDA, 1.16 g diethylenetriamine (DETA), 10 mg zinc acetate, and 40 mL DMF was dispersed in a 100 mL Teflon autoclave. The autoclave was then placed in a constant temperature oven at 160 °C for 5 h. After centrifugation and purification using a 1000 Da dialysis bag for 24 h, approximately 30 $mg{\cdot}mL^{-1}$ of PT-NCDs was obtained.

To synthesize g-CNQDs, 1.0 g urea, and 1.4 g sodium citrate were blended in a mortar, and the resultant mixture was transferred to a crucible. The crucible was heated to 180 °C for 120 min in a muffle furnace. After cooling, the resulting yellow powder was washed thoroughly. Following centrifugation and purification, an aqueous solution of g-CNQDs with a concentration of approximately 30 $mg{\cdot}mL^{-1}$ was obtained. The particle size of g-CNQDs was primarily concentrated around 5.4 ± 0.9 nm.

For CA-NCDs synthesis, 1.2 g citric acid (CA) and 0.675 mL DETA were heated in a 50 mL Teflon autoclave with 12 mL water, and the autoclave was placed at 180 °C for 6 h. After centrifugation and purification, approximately 30 $mg{\cdot}mL^{-1}$ CA-NCDs aqueous solution was obtained. High-resolution transmission electron microscopy (HR-TEM) image revealed that CA-NCDs have an average particle size of 5.1 ± 1.0 nm. The elemental composition of CDs is listed in Table 1.

Tauc plot formula: $h\nu = A(h\nu - Eg)^{n/2}$, where h is Planck's constant, ν is the photon's frequency, α is the absorption coefficient, E_g is the band gap, and A is a proportionality constant. The value of the exponent denotes the nature of the electronic transition, whether direct or indirect: for direct allowed transitions: $n = 1/2$, for indirect allowed transitions: $n = 2$.

The average photoluminescence lifetime of CDs is calculated as follows: $\tau = Rel\ 1\% * \tau_1 + Rel\ 2\% * \tau_2$. The results are list in Table 2.

2.3. Covalent assembly and characterization of cross-linked enzymes

The selection of mutant sites at positions 49(Y) and 266(E) and the construction of the plasmid were previously completed in our lab, previously [46]. Strains containing the recombinant plasmids were cultured in Luria-Bertani (LB) medium supplemented with 34 $\mu g{\cdot}mL^{-1}$ chloramphenicol, 50 $\mu g{\cdot}mL^{-1}$ ampicillin, and 100 $\mu g{\cdot}mL^{-1}$ kanamycin at 34 °C in a shaking incubator set to 220 rpm. When the OD_{600} reached 0.8, L-arabinose was added as an inducer to a final concentration of 0.2 % (*w/v*). Subsequently, 1 $mmol{\cdot}mL^{-1}$ *p*-AzF and 30 $mg{\cdot}mL^{-1}$ anhydrotetracycline (aTc) were added and cultured at 23 °C in a shaking incubator at 200 rpm for 16 h. The purified proteins, obtained using a Ni column, were analyzed by SDS-PAGE. The molecular weight of AKR-49-266 protein is about 32 kDa.

Table 1
Composition of CDs.

Sample	C1s	N1s	O1s
PT-NCDs	55.14 %	27.97 %	16.89 %
CA-NCDs	47.39 %	14.20 %	38.41 %
g-CNQDs	38.29 %	4.98 %	56.72 %

Table 2
The average lifetime of CDs.

Sample	τ_1 / ns	Rel $_1$ %	τ_2 / ns	Rel $_2$ %	$<\tau>$/ ns
PT-NCDs	3.65	87.02	8.74	12.98	4.31
CA-NCDs	2.55	11.07	13.79	88.93	12.55
g-CNQDs	4.11	46.11	9.8	53.89	7.18

For the bio-orthogonal crosslinking reaction, an 8 mM solution of dibenzocycloocta-a,6a-diene-5,11-diyne DBA in isopropanol was added to PBS buffer (1 mL, 0.1 mol L^{-1}, pH 7.0) containing the mutant. The molecular ratio of azide to the crosslinking agent is 1:2. The reaction mixture was placed in a microwave reactor with a cooling module (COOLMATE OPTION 542470-CEM, USA) and irradiated at 4–10 °C for 3 min. After centrifugation, the obtained CLEs were rinsed thrice with 1 M NaCl and deionized water to remove other proteins and cell debris.

To characterize the AKR-CLEs using a confocal laser scanning microscope (Zeiss LSM 900, CLSM), the fluorescent staining agent cy5-BisNTA-Ni was added to a final concentration of 1 mM and incubated at 4 °C for 48 h. After staining, the sample was washed by centrifugation with water, and a small drop of the micro-sample was placed on a glass slide. Once partially dried, the slide was covered with a coverslip. The CDs-CLEs sample was constructed by grafting CDs onto AKR-CLEs through self-assembly after shaking CDs and CLEs (at a molar ratio of 3:1) overnight. The AKR-CLEs and CDs-CLEs were observed with green and red fluorescence at 577–492 nm and 770–622 nm, respectively.

For transmission electron microscope (TEM, Hitachi HT-7700) observation, the CDs-CLEs were ultrasonically dispersed in a PBS buffer and dropped on a carbon film. After drying, the samples were observed under a 60.0 kV. For transmission electron microscope (TEM) observation, the AKR-CLEs were ultrasonically dispersed in a PBS buffer and precipitated by centrifugation. After drying, the samples were adhered in a conductive carrier, sprayed with gold powder for 20 s, and finally observed using a scanning electron microscope (JEOL, JSM-5600LV), and microscopic images were obtained under a 1.0 kV scanning electron microscope.

2.4. Synthesis of the electron mediator

The electron mediator was synthesized according to a published method [47]. $RhCl_3{\cdot}3H_2O$ (77 mg) and pentamethylcyclopentadiene (52 mg) were dissolved in 3 mL anhydrous methanol and then refluxed at 65 °C for 15 h under vigorous stirring in a nitrogen atmosphere. $[Cp^*Rh(bpy)(H_2O)]^{2+}$ **(M)** were prepared by mixing $[Cp^*RhCl_2]$ and two equivalents of bipyridine in methanol for 1 h. The final products were separated by crystallization in a methanol/diethyl ether mixture (1:5), and dried under vacuum overnight.

2.5. Photocatalytic regeneration of NADPH

For NADPH regeneration, the entire reaction was carried out at room temperature and ambient atmosphere. The reaction solution comprised 8 mM $NADP^+$, 1.8 mg mL^{-1} of CDs, 1 mM **M**, and 20 mM PBS (pH = 7.0) in a total volume of 2.5 mL. This solution was placed in a quartz cuvette and stirred for 15 min in the dark to reach adsorption/desorption equilibrium. It was irradiated with a 300 W Xe LED lamp (CEL-HXF300) with a ≥ 420 nm cut-off filter. Every 15 min, 50 μL of the reaction solution was taken out from the system, diluted to 1 mL with ultrapure water, and the absorbance at 340 nm was measured using a Shimadzu UV-1900i UV–vis spectrophotometer. The concentration of regenerated NADPH was calculated according to the Lambert–Beer law. Finally, AKR (2 mg mL^{-1}) and acetone (10 μL) were added to the diluted test solution to consume and quantify the biologically active 1,4-NADPH [48].

2.6. Photo-enzyme coupling catalytic synthesis of ketones

The 2.5 mL reaction system comprised 20 mM PBS buffer (pH 7.0), 8 mM $NADP^+$, 20 mM substrate, 1 mM **M**, 1.8 $mg{\cdot}mL^{-1}$ CDs, and 2 $mg{\cdot}mL^{-1}$ enzyme aggregates or enzyme. The reaction solution was placed in a 25 mL quartz reaction flask and stirred with a magnetic bar at photoreaction photoreactor (Fig. S1) with a cooling module maintaining the reaction temperature at 30 °C. Visible light irradiation was provided by a 300 W Xe lamp (CEL-HXF300) with a $\geq$ 420 nm cut-off filter. After 14 h, the reaction mixture was centrifuged. The supernatant was then collected, extracted with 2 mL ethyl acetate (EA), and washed three times with 2 mL water.

The isotope tracer experiment was performed following standard procedures, using D_2O as the solvent and *o*-chloroacetophenone as substrate. For recycling, the AKR-CLEs were isolated by centrifugation and then reused for (*S*)-1-(2-chlorophenyl) ethanol synthesis under standard photoenzymatic reaction conditions. (*S*)-1-(2-Chlorophenyl) ethanol yields were detected by reverse-phased flash chromatography (Agilent@C18) and their configuration was detected by normal-phase flash chromatography (CHIRALCEL@OD-H). Yield and isomer content of (*R*)-1-[3,5-bis(trifluoromethyl)phenyl]ethanol and (*S*)-3-chloro-1-phenylpropan-1-ol were detected by normal-phase flash chromatography (CHIRALCEL@OD-H). The separation and test conditions are provided in Supporting Information (SI).

3. Results and discussion

3.1. Structure characterization of CDs

The nitrogen-doped carbon dots named PT-NCDs were prepared using PTCDA and diethylenetriamine as the starting materials. Compared to typical carbon quantum dots (CA-NCDs) and C_3N_4 quantum dots (g-CNQDs) derived from citric acid and its analogs [49–51], PT-NCDs have a smaller particle size (average) with 3.9 ± 0.5 nm (**Fig. 1a** and **d**). Similar to other CDs, the PT-NCDs can be well dispersed in water. Surface topology analysis also reveals that the CDs display clear lattice fringes with a *d*-spacing of 0.21 nm at a 5 nm resolution corresponding to the (100) crystal plane of graphene (Fig. 1a and c) [52], while CA-NCDs displayed amorphous structures (Fig. 1b).

The PT-NCDs are mainly composed of carbon (55.14 %), nitrogen (27.97 %), and oxygen (16.89 %) (Fig. 2a and Table 1). The carbon valence states are identified as C═C (284.55 eV), C-N/C-O (285.62 eV), and C═O (287.56 eV) (Fig. 2b). For N 1 s spectra, the nitrogen valence states are shown as pyridinic nitrogen (398.60 eV), graphitic nitrogen (399.69 eV), and amino (401.88 eV) (Fig. 2c) [44]. Most importantly, PT-NCDs demonstrate the highest nitrogen content (Fig. 2c) [52]. In the FT-IR spectra of the CDs (Fig. 2d), the 3500 ~ 3200 cm^{-1} region corresponds to the stretching vibration of amino groups ($^-NH_2$) and hydroxyl (-OH), while the ~1630 cm^{-1} represents carbonyl (C=O) stretching vibrations. From this, it's easy to understand why the nitrogen-doped CDs are soluble in water [53]. Besides, breathing bands at 807 and 894 cm^{-1} reconfirm the existence of the *s*-triazine structure of graphitic carbon nitride [54].

Furthermore, Raman spectrum analysis of PT-NCDs exhibits sharp peaks near 1385 cm^{-1} and 1580 cm^{-1}. It can be attributed to disordered and vibrated sp^3 structure (D band) and in-plane graphite sp^2 structure (G band), respectively (*e.g.* Fig. 2f). Other CDs have strong fluorescent signals but lack a distinct Raman signal. X-ray diffraction (XRD) spectroscopy was used to characterize the structure of the CDs, showing broad peaks at 24° and 27.3° that correspond to the planes of graphite (002), indicative of varying degrees of graphitization, as shown in Fig. 2e [42]. In addition, a peak of zeta potential ($^-$36.4 mV) for PT-NCDs indicates the presence of carboxyl groups on its surface (Fig. 2g). The negative charge moieties on the surface impart excellent solubility of carbon dots in water.

3.2. Optical and photoelectrochemical properties of CDs

Corresponding UV–vis absorption spectra demonstrate that the CA-NCDs and g-CNQDs have major absorption bands at the ultraviolet-to-violet region, consistent with previous reports (Fig. 3a) [30], whereas PT-NCDs show absorption covering all visible regions from 400 to 800 nm. In particular, the wide absorption peak located at 500 nm, can be attributed to n → π* leaps of heterocyclic, C═O, or C—N groups (Fig. 3c). According to the Tauc plot, the band gap energies (E_g) of PT-NCDs, CA-NCDs and g-CNQDs are calculated to be 2.31, 3.17 and 2.74 eV, respectively (Fig. 3b). These results determined that only PT-NCDs and g-CNQDs can be excited by visible light. In addition, PT-NCDs and g-CNQDs exhibit excitation-independent photoluminescent emission (Fig. 3d-e). The g-CNQDs and PT-NCDs have relatively long fluorescence lifetimes, 7.18 ns and 4.31 ns, respectively (Fig. 3f), implying efficient electron transfer efficiency and prolonged photogenerated carrier lifetimes [26].

To further insight into the band structure of different CDs, valance band X-ray photoelectron spectroscopy (VB XPS) analysis was carried out. The valance band (VB) potentials for PT-NCDs and CA-NCDs are

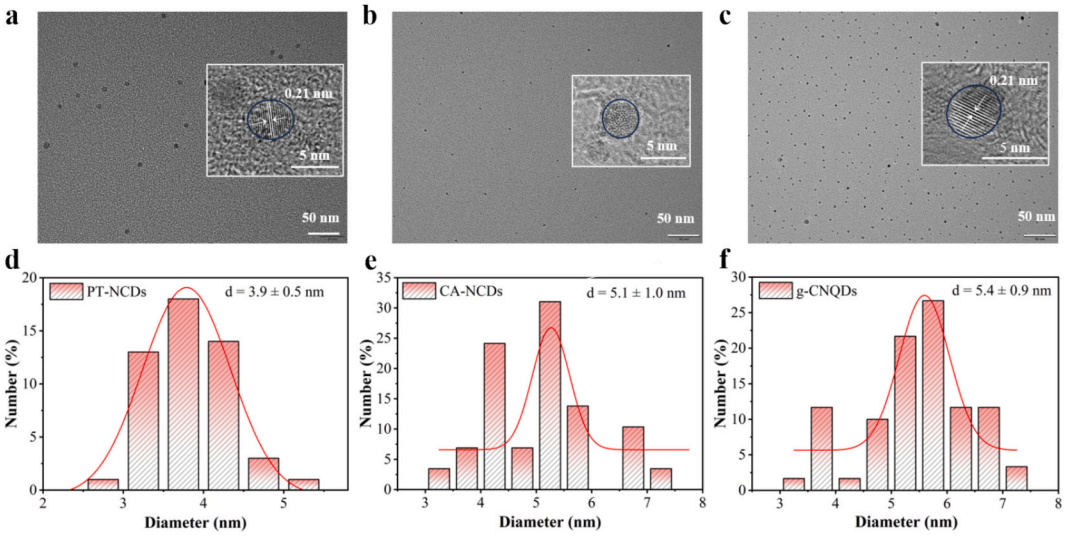

Fig. 1. Transmission electron microscopy (TEM) and high-resolution transmission electron microscopy (HRTEM, inset) images of the (a) PT-NCDs, (b) CA-NCDs, (c) g-CNQDs; Size distribution of (d) PT-NCDs, (e) CA-NCDs, (f) g-CNQDs.

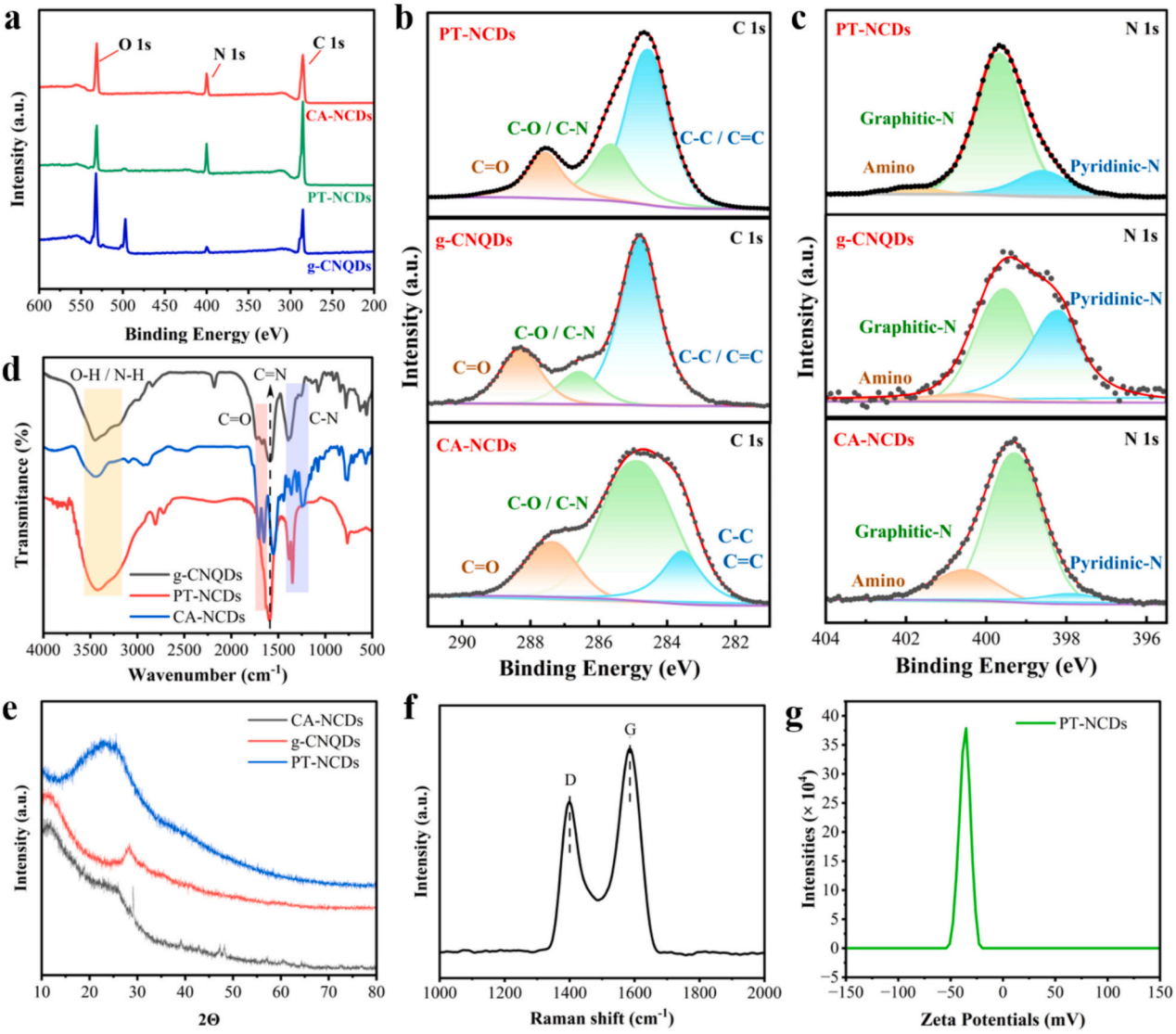

Fig. 2. Chemical structural analysis of CDs: (a) XPS survey spectra of CDs; High-resolution (b) C 1 s, (c) N 1 s XPS spectra of CDs; (d) FT-IR spectra of CDs; (e) XRD patterns of CDs; (f) Raman spectrum of PT-NCDs; (g) Zeta potential of PT-NCDs.

measured as 1.58 eV and 1.50 eV *versus* the normal hydrogen electrode (NHE), respectively (Fig. 4a). Mott-Schottky measurements of g-CNQDs were also performed to investigate their charge potentials, revealing a positive slope in the Mott-Schottky curve (Fig. 4b). Similar to typical g-C_3N_4, the conduction band (CB) and VB positions of g-CNQDs are determined to be 1.04 V and 1.70 (*vs* NHE), respectively [55]. Based on the preceding data, an energy level diagram for the CDs is conducted (Fig. 4c) [56]. The broad energy band of CA-NCDs renders them unsuitable as photocatalysts. In contrast, the g-CNQDs and PT-NCDs can be excited under visible light irradiation to produce e^-/ h^+ pairs. Specifically, the VB potentials of g-CNQDs and PT-NCDs are more positive than the oxidation potential of H_2O [$E(O_2/H_2O) = 1.23$ V], suggesting that the photogenerated hole in the VB is capable of oxidizing H_2O.

3.3. Light-driven regeneration of NADPH by CDs

The inclusion of electron and proton mediator $[Cp^*Rh(bpy)(H_2O)]^{2+}$ (**M**) is generally compulsory to integrate the hole/electron-transfer chain for highly selective regeneration of 1,4-NADPH. Thus, to investigate its efficiency, we performed the photocatalytic NADPH regeneration system in the presence of **M** and CDs without an additional electron donor. It can be observed that nothing occurred during the period of darkness (Fig. 4d). Upon illumination, PT-NCDs gave the highest synthesis rate for active NADPH, attributed to their good visible light absorption and energy conversion capabilities. The yield of NADPH reached 55.7 % at 90 min, which is 2.23 and 6.26 times greater than yields catalyzed by g-CNQDs and CA-NCDs, respectively (Fig. 4d).

3.4. Light-driven redox biocatalysis using CDs-enzyme hybrid catalyst

Initially, photo-enzymatic catalysis was performed under visible light irradiation, using CDs as the sole photocatalyst, crosslinked aldo-keto reductase (AKR-CLEs) as the biocatalyst, and **M** as the electron mediator. The utilization of AKR-CLEs aims to improve enzyme stability while omitting the tedious purification step. The biocatalyst was obtained through a click reaction between the azide on the non-canonical amino acids (ncAAs) of the AKR mutant and alkynyl groups of cross-linker, allowing their further interaction with CDs to afford CLEs-CDs composites (Fig. 5a). The expression of AKR mutant was confirmed by SDS-PAGE analysis (Fig. S5). The target protein yields in an average of 97 mg·L^{-1} and obtains 0.91 ± 0.021 U·mg^{-1} specific enzyme activity. After cross-linking, the AKR-CLEs maintained 0.94 ± 0.028 U·mg^{-1} activity, which is comparable to the activity of wild AKR (Table S1). The use of cross-linked enzymes is expected to have better chemical stability

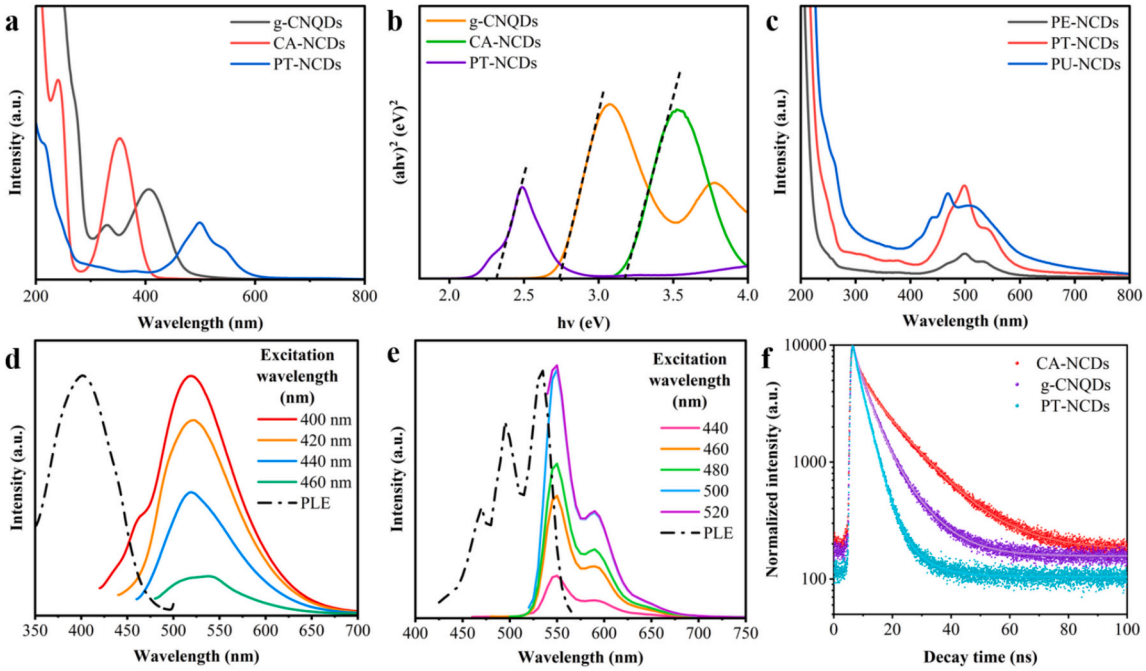

Fig. 3. Optical characterization of CDs: (a) Absorbance spectra of CDs; (b) Tauc plots of CDs; (c) Absorbance spectra of P-NCDs; Fluorescent emission map and ex-em spectrum of (d) g-CNQDs, (e) PT-NCDs; (f) Fitting Time-resolved photoluminescence decays spectra of CDs.

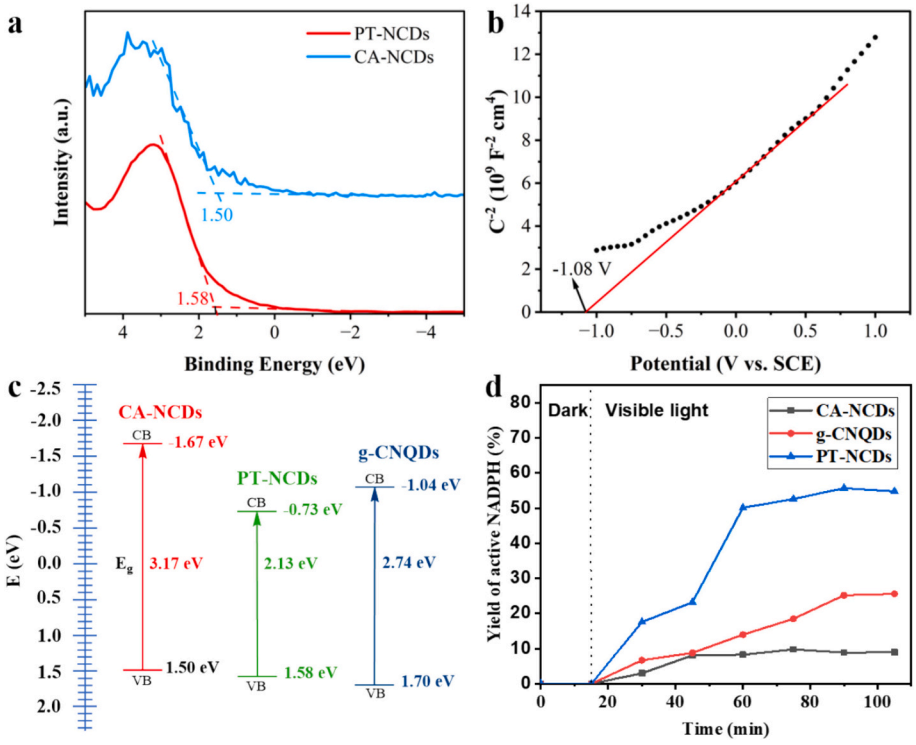

Fig. 4. Characterization of the electronic structure of CDs: (a) Valence band spectra measured by XPS; (b) Mott-Schottky curve of g-CNQDs; (c) Band structures of CDs; (d) Photocatalytic yield of NADPH using different CDs.

and recyclability in catalysis.

It is difficult to distinguish the AKR-CLEs and CDs in the TEM image of CDs-CLEs composites (Fig. 5b). To assess the interaction of PT-NCDs and enzyme, a labeling strategy was applied using a short peptide tag and a recognition of small molecular probes to visualize AKR-CLEs. When AKR-CLEs were mixed with the fluorescent probe, '-Cy5-Bisnta-Ni', the His-Tag present on the AKR variant specifically bound to the Cy5-Bisnta-Ni, resulting in red fluorescence in the 770–622 nm range after light stimulation. SEM and CLSM morphological characterization reveal AKR-CLEs were well aggregated, with maximum diameters close to 10 μm (Fig. 5c-d). The PT-NCDs and AKR-CLEs launched green and red fluorescence, respectively, when the PT-NCDs-CLEs were excited at 488 nm and 640 nm (Fig. 5e-f). Co-localization fluorescence analysis of the bio-organic hybrids afforded scatter plots of fluorescence intensity of

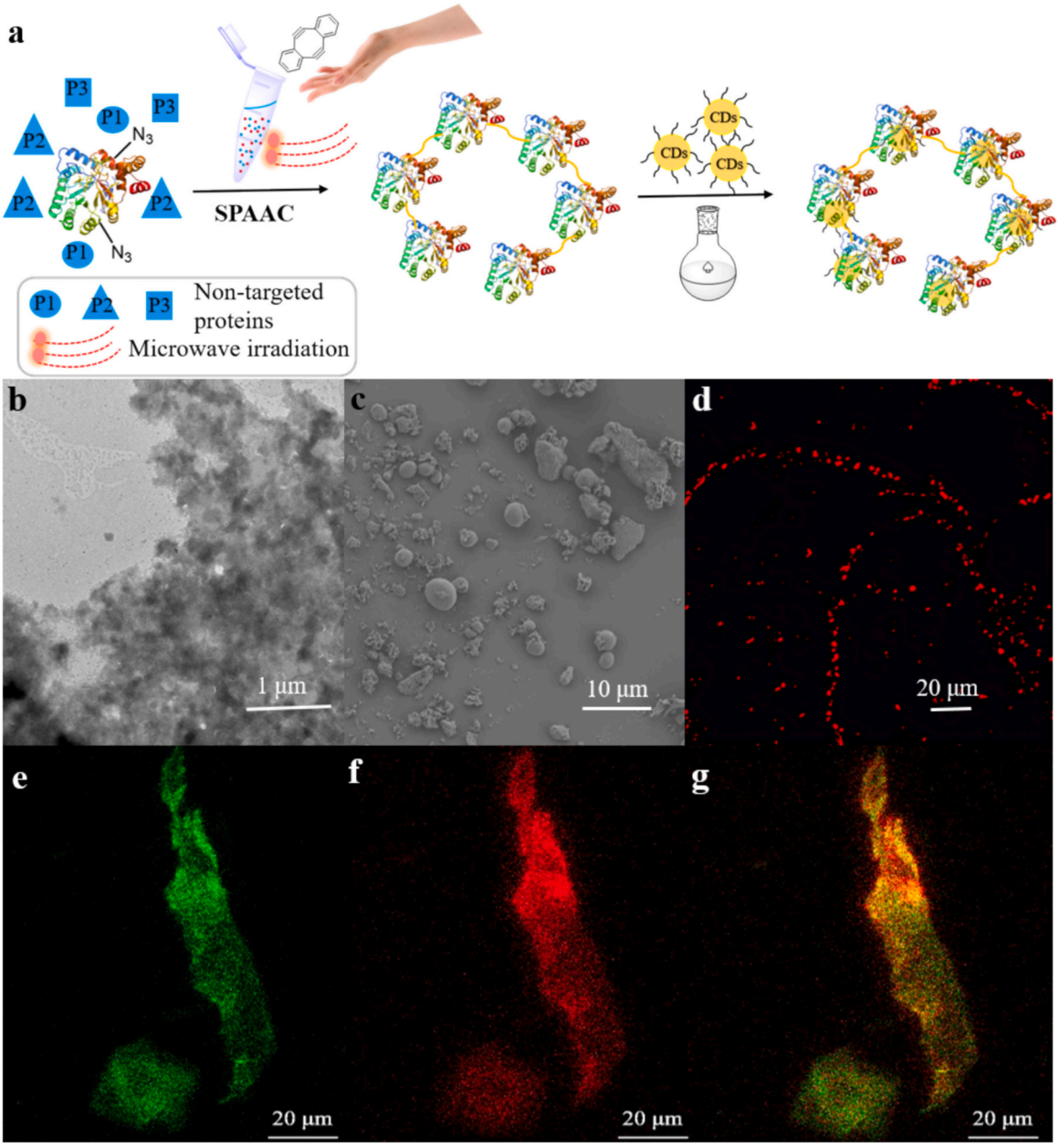

Fig. 5. (a) Schematic preparation process of CDs-CLEs composites; (b) TEM image of AKR-CLEs with PT-NCDs attached; (c) SEM image of AKR-CLEs; (d) CLSM image of AKR-CLEs. CLSM images of PT-NCDs-CLEs after irradiation by 488 nm (e), irradiation by 640 nm (f), and their co-localization scatterplot of red and green pixel intensity (g). (For interpretation of the references to colour in this figure legend, the reader is referred to the web version of this article.)

red and green channels (Fig. 5g). The green fluorescence is concentrated in the red fluorescence regions, suggesting a strong affinity between PT-NCDs and AKR-CLEs (Fig. 5g).

Hydrogenation of *o*-chloroacetophenone requires AKR and one equivalent of NADPH cofactor. Based on the thermodynamics principle, upon excitation by visible light, CDs and **M** transfer the electrons and protons from water to $NADP^+$ to regenerate NADPH *in situ*. As NADPH is consumed, AKR-CLEs are active to carry out the asymmetric hydrogenation of ketone and release $NADP^+$, completing the catalytic cycle (Fig. 6a). First, the reaction did not occur in the absence of enzymes or CDs (Fig. 6b and Fig. S9). We then confirmed the feasibility of the catalytic concept by replacing water with D_2O, using AKR-CLEs and PT-NCDs as the biocatalyst and photocatalyst, respectively. The system produced 65.3 % of (*S*)-1-(2-chlorophenyl) ethanol with 99.99 % enantiomeric excess (ee) under 20 mM substrate concentration (Fig. 6b and Fig. S10–11). The positive ion mode high-resolution mass spectroscopy (HRMS) analysis of the product from isotope tracer experiments shows that it is only deuterated 2-chlorophenylethanol with molecular formula $C_8H_7D_2OCl$ corresponding molecular weight 158.0438 (Fig. S6). Under negative ion mode, the product lost one D-atom corresponding to a molecular weight of 156.0329 (Fig. S7). These results imply that water is the hydrogen donor.

Next, the photocatalytic reduction capabilities of other CDs were compared in the absence of extra sacrificial reductants. Notably, these reactions gave 29.5 % and 18.6 % yields with the g-CNQDs and CA-NCDs as the photosensitizer, respectively (Fig. 6b and Fig. S12). These results demonstrate that PT-NCDs exhibit the highest photocatalytic efficiency in water splitting for biocatalytic reduction. Lower efficiency observed for g-CNQDs and CA-NCDs is likely due to their wider band gaps [57]. HPLC analysis confirmed that all the reactions achieved 99.99 % ee, indicating that the photo-enzyme coupling catalysis retained AKR's high enantioselectivity (Fig. 6b and Fig. S12). Besides, the reaction yield was

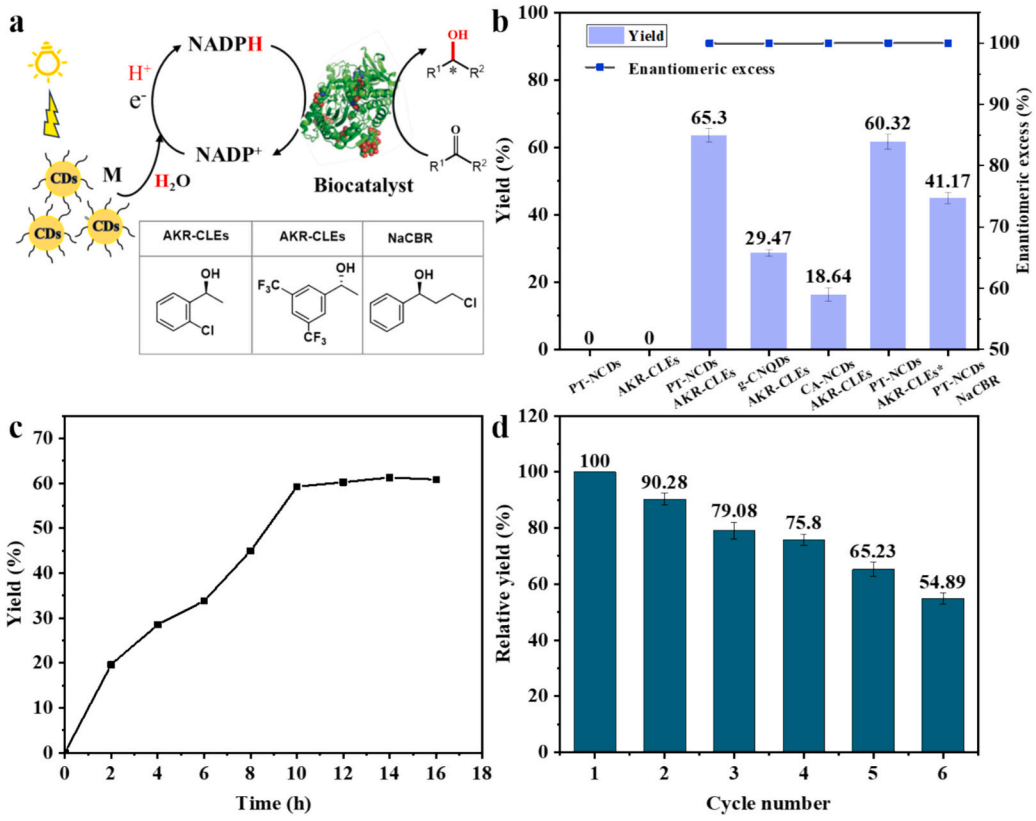

Fig. 6. Reaction conditions: a 2.5 mL reaction system consisting of 20 mM PBS buffer (pH 7.0), 8 mM $NADP^+$, 20 mM substrate, 1 mM **M**, 1.8 mg·mL^{-1} CDs, and 2 mg·mL^{-1} biocatalyst, under visible light with a wavelength ≥ 420 nm for 14 h. (a) Scheme of one-pot produce chiral alcohols by photo-enzymatic catalysis method; (b) Yields of alcohols with different reaction conditions including no enzyme, no CDs or using different CDs for (*S*)-1-(2-chlorophenyl) ethanol synthesis, using PT-NCDs/AKR-CLEs for (*R*)-1-[3,5-bis(trifluoromethyl)phenyl]ethanol synthesis, and using PT-NCDs/NaCBR for (*S*)-3-chloro-1-phenylpropan-1-ol synthesis; (c) The yield of (*S*)-1-(2-chlorophenyl) ethanol when PT-NCDs were used as the photocatalyst; (d) The recycling of AKR-CLEs.

monitored to get more insights into the photo-enzyme coupling system. It can be seen that the reaction rate was relatively fast in the early stages, and after 10 h, the yield increased very little (Fig. 6c, Fig. S13 and Table S2).

In this study, small-sized CD nanomaterials cannot be reused for separation difficulties, whereas micron-sized AKR-CLEs can. The recyclability of AKR-CLEs with *o*-chloroacetophenone as the model substrate was also measured. As a result of catalytic efficiency tests, AKR-CLEs maintained 54.9 % of their original catalytic activity and excellent enantioselectivity (99.99 %) even after six cycles of use in the photo-enzymatic reduction (Fig. 6d and Fig. S10, S12). It's worth noting that our operation is carried out in small batches. The post-processing steps may result in enzyme loss, leading to a later decrease in catalytic efficiency. However, the impact may be eliminated when the reaction scale is increased.

We also examine the applicability of the PT-NCDs-AKR photo-enzymatic cascade catalysis method. (*R*)-1-[3,5-Bis(trifluoromethyl)phenyl] ethanol [(*R*)-3,5-BTPE] is a key intermediate for Aprepitant, a typical anti-nausea drug to cancer patients after chemotherapy. It can be selectively synthesized by AKR in the presence of NADPH from 3,5-bis (trifluoromethyl)acetophenone [58–61]. Using the *in situ* regeneration system, (*R*)-3,5-BTPE was obtained in a 60.3 % yield with 99.99 % ee (Fig. 6b and Fig. S14). Above strategy is theoretically acceptable for other NADPH-dependent enzymes with photostable substrate and product. For instance, a carbonyl reductase from *Novosphingobium aromaticivorans* (NaCBR) [62]. The combination of PT-NCDs and NaCBR produced a 41.2 % yield of (*S*)-3-chloro-1-phenyl-1-propanol with 99.98 % ee, which is a valuable chemical for the synthesis of antidepressive Fluoxetine (Fig. 6b and Fig. S15).

4. Conclusions

In conclusion, we have demonstrated that visible-light-responsive CDs can drive water splitting to enable photo-enzymatic synthesis of chiral alcohols, with cofactors generated *in situ via* photocatalysis. The CDs' properties vary depending on the carbon source and reaction conditions. PT-NCDs with a smaller size exhibit the best visible photocatalytic reduction activity, yielding 65.3 % and 99.99 % ee for (*S*)-1-(2-chlorophenyl) ethanol in the photoenzymatic reduction with AKR-CLEs as the biocatalyst. This coupling effectively preserves enzyme activity, allowing AKR-CLEs to be reused multiple times while maintaining good catalytic efficiency under complex photochemical conditions. Similarly, a 60.3 % yield and 99.99 % ee for (*R*)-1-[3, 5-bis (trifluoromethyl)] phenyl ethanol and a 41.2 % yield and 99.99 % ee for (*S*)-3-chloro-1-phenyl-1-propanol suggest wide applicability. This high enantioselectivity is attributed to photo-enzymatic catalysis rather than direct photocatalytic reduction. However, free CDs are far from industrial applications requiring continuous flow or fixed beds. Future research should prioritize developing functionalized CDs for the integration of the entire photoenzymatic catalysis system.

CRediT authorship contribution statement

Yi Zhang: Validation, Methodology. **Roger A. Sheldon:** Writing – review & editing, Supervision. **Anming Wang:** Writing – review & editing, Visualization, Supervision, Project administration, Funding acquisition, Conceptualization.

Declaration of competing interest

The authors declare that they have no known competing financial interests or personal relationships that could have appeared to influence the work reported in this paper.

Acknowledgements

This work was supported by the National Natural Science Foundation of China (22078079, 22378091, 22378092, 22178078), the Natural Science Foundation of Zhejiang Province (LY18B060009), and the Program for Postgraduates in Innovation Practice and Service for Locality in HZNU (2022).

Appendix A. Supplementary data

Supplementary data to this article can be found online at https://doi.org/10.1016/j.ijbiomac.2024.139444.

Data availability

Data will be made available on request.

References

[1] G. Qu, A. Li, C.G. Acevedo-Rocha, Z. Sun, M.T. Reetz, Angew. Chem. Int. Ed. 59 (2020) 13204–13231, https://doi.org/10.1002/anie.201901491.
[2] J. Guo, M. Suástegui, K.K. Sakimoto, V.M. Moody, G. Xiao, D.G. Nocera, N.S. Joshi, Science 362 (2018) 813–816, https://doi.org/10.1126/science.aat9777.
[3] T. Peng, J. Tian, Y. Zhao, X. Jiang, X. Cheng, G. Deng, Q. Zhang, Z. Wang, J. Yang, Y. Chen, Angew. Chem. Int. Ed. 61 (2022) e202209272, https://doi.org/10.1002/anie.202209272.
[4] S. Li, J. Shi, S. Liu, W. Li, Y. Chen, H. Shan, Y. Cheng, H. Wu, Z. Jiang, Chin. J. Catal. 44 (2023) 96–110, https://doi.org/10.1016/S1872-2067(22)64154-8.
[5] X. Huang, B. Wang, Y. Wang, G. Jiang, J. Feng, H. Zhao, Nature 584 (2020) 69–74, https://doi.org/10.1038/s41586-020-2406-6.
[6] X. Wang, T. Saba, H.H.P. Yiu, R.F. Howe, J.A. Anderson, J. Shi, Chem 2 (2017) 621–654, https://doi.org/10.1016/j.chempr.2017.04.009.
[7] Z.C. Litman, Y. Wang, H. Zhao, J.F. Hartwig, Nature 560 (2018) 355–359, https://doi.org/10.1038/s41586-018-0413-7.
[8] M.A. Emmanuel, S.G. Bender, C. Bilodeau, J.M. Carceller, J.S. DeHovitz, H. Fu, Y. Liu, B.T. Nicholls, Y. Ouyang, C.G. Page, T. Qiao, F.C. Raps, D.R. Sorigué, S.-Z. Sun, J. Turek-Herman, Y. Ye, A. Rivas-Souchet, J. Cao, T.K. Hyster, Chem. Rev. 123 (2023) 5459–5520, https://doi.org/10.1021/acs.chemrev.2c00767.
[9] N. Sun, J. Huang, J. Qian, T. Zhou, J. Guo, L. Tang, W. Zhang, Y. Deng, W. Zhao, G. Wu, R. Liao, X. Chen, F. Zhong, Y. Wu, Nature 611 (2022) 715–720, https://doi.org/10.1038/s41586-022-05342-4.
[10] X. Pei, Z. Luo, L. Qiao, Q. Xiao, P. Zhang, A. Wang, R.A. Sheldon, Chem. Soc. Rev. 51 (2022) 7281–7304, https://doi.org/10.1039/D1CS01004B.
[11] J. Zhang, R. Wang, Z. Luo, D. Jia, H. Chen, Q. Xiao, P. Zhang, X. Pei, A. Wang, Materials Chemistry Frontiers 6 (2022) 182–193, https://doi.org/10.1039/d1qm01285a.
[12] P. Zhang, W. Dong, Y. Zhang, L.-N. Zhao, H. Yuan, C. Wang, W. Wang, H. Wang, H. Zhang, J. Liu, Chinese Journal of Catalysis 54 (2023) 188–198, https://doi.org/10.1016/S1872-2067(23)64523-1.
[13] J. Liu, N. Ma, W. Wu, Q. He, Chem. Eng. J. 393 (2020) 124719, https://doi.org/10.1016/j.cej.2020.124719.
[14] S. Liu, J. Shi, J. Jia, Y. Yang, S. Zhang, D. Yang, Y. Chen, S. Li, Z. Jiang, ACS Catalysis 13 (2023) 14233–14240, https://doi.org/10.1021/acscatal.3c03180.
[15] U. Bat-Erdene, J.M. Billingsley, W.C. Turner, B.R. Lichman, F.M. Ippoliti, N. K. Garg, S.E. O'Connor, Y. Tang, ACS Catal. 11 (2021) 9898–9903, https://doi.org/10.1021/acscatal.1c02267.
[16] C. Zhang, H. Zhang, J. Pi, L. Zhang, A. Kuhn, Angew. Chem. Int. Ed. (2021) 61, https://doi.org/10.1002/anie.202111804.
[17] S. Li, Y. Cheng, Y. Chen, J. Li, Y. Sun, J. Shi, Z. Jiang, Appl. Catal. Environ. 317 (2022) 121772, https://doi.org/10.1016/j.apcatb.2022.121772.
[18] F. Xie, H. Jia, C.K.T. Wun, X. Huang, Y. Chai, C.C. Tsoi, Z. Pan, S. Zhu, K. Ren, T.W. B. Lo, Y. Zhu, X. Zhang, ACS Sustain. Chem. Eng. 11 (2023) 11002–11011, https://doi.org/10.1021/acssuschemeng.3c00361.
[19] Z. Zhang, J. Tong, X. Meng, Y. Cai, S. Ma, F. Huo, J. Luo, B. Xu, S. Zhang, M. Pinelo, ACS Sustainable Chemistry & Engineering 9 (2021) 11503–11511, https://doi.org/10.1021/acssuschemeng.1c03737.
[20] V.M. Badiani, C. Casadevall, M. Miller, S.J. Cobb, R.R. Manuel, I.A.C. Pereira, E. Reisner, J. Am. Chem. Soc. 144 (2022) 14207–14216, https://doi.org/10.1021/jacs.2c04529.
[21] C. Zhang, H. Zhang, J. Pi, L. Zhang, A. Kuhn, Angew. Chem. Int. Ed. 61 (2022) e202111804, https://doi.org/10.1002/anie.202111804.
[22] M. Mifsud, S. Gargiulo, S. Iborra, I.W.C.E. Arends, F. Hollmann, A. Corma, Nat. Commun. 5 (2014) 3145, https://doi.org/10.1038/ncomms4145.
[23] K. Köninger, Á. Gómez Baraibar, C. Mügge, C.E. Paul, F. Hollmann, M. M. Nowaczyk, R. Kourist, Angew. Chem. Int. Ed. 55 (2016) 5582–5585, https://doi.org/10.1002/anie.201601200.
[24] D. Mersch, C. Lee, J.Z. Zhang, K. Brinkert, J.C. Fontecilla-Camps, A.W. Rutherford, E. Reisner, J. Am. Chem. Soc. 137 (2015) 8541–8549, https://doi.org/10.1021/jacs.5b03737.
[25] B. Zhang, B. Wang, E.V. Ushakova, B. He, G. Xing, Z. Tang, A.L. Rogach, S. Qu, Small 19 (2022) 2204158, https://doi.org/10.1002/smll.202204158.
[26] X. Yang, L. Sheng, Y. Ye, J. Sun, S. Geng, D. Ning, Y. Zhang, X. Sun, Chem. Eng. J. 474 (2023) 145771, https://doi.org/10.1016/j.cej.2023.145771.
[27] G.A.M. Hutton, B. Reuillard, B.C.M. Martindale, C.A. Caputo, C.W.J. Lockwood, J. N. Butt, E. Reisner, J. Am. Chem. Soc. 138 (2016) 16722–16730, https://doi.org/10.1021/jacs.6b10146.
[28] Z. Wang, Y. Zhang, S. Zhang, M. Ge, H. Zhang, S. Wang, Z. Chen, S. Li, C. Yang, J. Colloid Interface Sci. 629 (2023) 12–21, https://doi.org/10.1016/j.jcis.2022.09.044.
[29] M.V. Pavliuk, M. Lorenzi, D.R. Morado, L. Gedda, S. Wrede, S.H. Mejias, A. Liu, M. Senger, S. Glover, K. Edwards, G. Berggren, H. Tian, J. Am. Chem. Soc. 144 (2022) 13600–13611, https://doi.org/10.1021/jacs.2c03882.
[30] G.A.M. Hutton, B.C.M. Martindale, E. Reisner, Chem. Soc. Rev. 46 (2017) 6111–6123, https://doi.org/10.1039/c7cs00235a.
[31] M. Han, S. Zhu, S. Lu, Y. Song, T. Feng, S. Tao, J. Liu, B. Yang, Nano Today 19 (2018) 201–218, https://doi.org/10.1016/j.nantod.2018.02.008.
[32] X. Guan, Z. Li, X. Geng, Z. Lei, A. Karakoti, T. Wu, P. Kumar, J. Yi, A. Vinu, Small 19 (2023) 2207181, https://doi.org/10.1002/smll.202207181.
[33] H. Wu, S. Lu, B. Yang, Accounts of Materials Research 3 (2022) 319–330, https://doi.org/10.1021/accountsmr.1c00194.
[34] H. Yu, Y. Zhao, C. Zhou, L. Shang, Y. Peng, Y. Cao, L. Wu, C. Tung, T. Zhang, J. Mater. Chem. A 2 (2014) 3344–3351, https://doi.org/10.1039/C3TA14108J.
[35] C. Rosso, G. Filippini, M. Prato, ACS Catalysis 10 (2020) 8090–8105, https://doi.org/10.1021/acscatal.0c01989.
[36] C. Baslak, S. Demirel, A. Kocyigit, H. Alatli, M. Yildirim, Mater. Sci. Semicond. Process. 147 (2022) 106738, https://doi.org/10.1016/j.mssp.2022.106738.
[37] J. Wang, J. Jiang, F. Li, J. Zou, K. Xiang, H. Wang, Y. Li, X. Li, Green Chem. 25 (2023) 32–58, https://doi.org/10.1039/D2GC03160D.
[38] Y. Zhao, L. Yu, Y. Deng, K. Peng, Y. Yu, X. Zeng, Ceram. Int. 49 (2023) 16647–16651, https://doi.org/10.1016/j.ceramint.2023.02.025.
[39] N. Choi, C. Tang, Y. Park, A. Du, G.A. Ayoko, Y. Hwang, S. Chae, Sep. Purif. Technol. 350 (2024) 127836, https://doi.org/10.1016/j.seppur.2024.127836.
[40] B.C.M. Martindale, G.A.M. Hutton, C.A. Caputo, S. Prantl, R. Godin, J.R. Durrant, E. Reisner, Angew. Chem. Int. Ed. 56 (2017) 6459–6463, https://doi.org/10.1002/anie.201700949.
[41] H. Song, Y. Li, L. Shang, Z. Tang, T. Zhang, S. Lu, Nano Energy 72 (2020) 104730, https://doi.org/10.1016/j.nanoen.2020.104730.
[42] L. Đorđević, F. Arcudi, M. Cacioppo, M. Prato, Nat. Nanotechnol. 17 (2022) 112–130, https://doi.org/10.1038/s41565-021-01051-7.
[43] K. Gao, X. Gao, W. Zhu, C. Wang, T. Yan, F. Fu, J. Liu, C. Liang, Q. Li, Chem. Eng. J. 406 (2021) 127155, https://doi.org/10.1016/j.cej.2020.127155.
[44] Y. Liu, J.H. Lei, G. Wang, Z. Zhang, J. Wu, B. Zhang, H. Zhang, E. Liu, L. Wang, T. Liu, G. Xing, D. Ouyang, C. Deng, Z. Tang, S. Qu, Adv. Sci. 9 (2022) 2202283, https://doi.org/10.1002/advs.202202283.
[45] Y. Li, X. Zhang, D. Liu, J. Photochem. Photobiol. C Photchem. Rev. 48 (2021) 100436, https://doi.org/10.1016/j.jphotochemrev.2021.100436.
[46] L. Qiao, Z. Luo, R. Wang, X. Pei, S. Wu, H. Chen, T. Xie, R.A. Sheldon, A. Wang, Green Chem. 25 (2023) 7547–7555, https://doi.org/10.1039/D3GC01898A.
[47] J. Liu, X. Ren, C. Li, M. Wang, H. Li, Q. Yang, Appl. Catal. Environ. 310 (2022) 121314, https://doi.org/10.1016/j.apcatb.2022.121314.
[48] M. Wang, H. Dai, Q. Yang, Angew. Chem. Int. Ed. 62 (2023) e202309929, https://doi.org/10.1002/anie.202309929.
[49] W. Liu, C. Jiang, J. Feng, L. Zhang, Q. Hou, X. Ji, Int. J. Biol. Macromol. 260 (2024) 129587, https://doi.org/10.1016/j.ijbiomac.2024.129587.
[50] R. Sendão, M.d.V.M.d. Yuso, M. Algarra, J.C.G. Esteves da Silva, L. Pinto da Silva, J. Clean. Prod. 254 (2020) 120080, https://doi.org/10.1016/j.jclepro.2020.120080.
[51] P. Zhao, B. Jin, Q. Zhang, R. Peng, Appl. Surf. Sci. 586 (2022) 152792, https://doi.org/10.1016/j.apsusc.2022.152792.
[52] Q. Zhang, F. Wang, R. Wang, J. Liu, Y. Ma, X. Qin, X. Zhong, Advanced Science 10 (2023) 2207566, https://doi.org/10.1002/advs.202207566.
[53] G.A. Hutton, B. Reuillard, B.C. Martindale, C.A. Caputo, C.W. Lockwood, J.N. Butt, E. Reisner, J. Am. Chem. Soc. 138 (2016) 16722–16730, https://doi.org/10.1021/jacs.6b10146.
[54] P. Yadav, S.T. Nishanthi, B. Purohit, A. Shanavas, K. Kailasam, Carbon 152 (2019) 587–597, https://doi.org/10.1016/j.carbon.2019.06.045.
[55] J. Fu, J. Yu, C. Jiang, B. Cheng, Adv. Energy Mater. 8 (2018) 1701503, https://doi.org/10.1002/aenm.201701503.
[56] T.-F. Yeh, C. Teng, S. Chen, H. Teng, Adv. Mater. 26 (2014) 3297–3303, https://doi.org/10.1002/adma.201305299.
[57] S. Nishioka, F.E. Osterloh, X. Wang, T.E. Mallouk, K. Maeda, Nature Reviews Methods Primers 3 (2023) 43, https://doi.org/10.1038/s43586-023-00234-x.
[58] Y.C. Yin, R. Wang, J. Zhang, Z.Y. Luo, Q.J. Xiao, T. Xie, X.L. Pei, P. Gao, A. M. Wang, ACS Appl. Mater. Interfaces 13 (2021) 41454–41463, https://doi.org/10.1021/acsami.1c11050.
[59] Y. Lu, J.M. Wang, H.B. Xu, C.Y. Zhang, P.P. Cheng, L.H. Du, L. Tang, J.H. Li, Z. M. Ou, Molecules 27 (2022) 7331, https://doi.org/10.3390/molecules27217331.

[60] K.L. Chen, K.F. Li, J. Deng, B.Q. Zhang, J.P. Lin, D.Z. Wei, Microb. Cell Fact. 15 (2016) 191, https://doi.org/10.1186/s12934-016-0585-5.
[61] H.M. Li, J. Moncecchi, M.D. Truppo, Org. Process Res. Dev. 19 (2015) 695–700, https://doi.org/10.1021/op5003215.
[62] Y. Tang, G. Zhang, Z. Wang, D. Liu, L. Zhang, Y. Zhou, J. Huang, F. Yu, Z. Yang, G. Ding, Bioresour. Technol. 250 (2018) 457–463, https://doi.org/10.1016/j.biortech.2017.10.097.